Experimental Evidence for the Existence of Non-*exo*-Anomeric Conformations in Branched Oligosaccharides: NMR Analysis of the Structure and Dynamics of Aminoglycosides of the Neomycin Family

Juan Luis Asensio,*[a] Ana Hidalgo,[a] Igor Cuesta,[a] Carlos González,[b] Javier Cañada,[c] Cristina Vicent,[a] Jose Luis Chiara,[a] Gabriel Cuevas,[c, d] and Jesús Jiménez-Barbero[c]

Abstract: It is commonly known that the *exo*-anomeric effect is a major factor governing the conformational behavior of naturally occurring oligosaccharides. Conformational flexibility in these molecules mainly concerns the aglycon ψ angle since ϕ is restricted by this stereoelectronic effect. In fact, to the best of our knowledge no case of a natural glycoside adopting a non-*exo*-anomeric conformation in solution has yet been reported. With respect to the flexibility among naturally occurring carbohydrates, branched type oligosaccharides including sugar residues glycosidated at contiguous positions (such as blood type carbohydrate antigens Lewis X) have been considered as the paradigm of rigid saccharides—the rigidity being enhanced by van der Waals interactions. Herein, we demonstrate unambiguously that both common beliefs are not to be generalized. For example in neomycin B, a branched oligosaccharide antibiotic, a large number of non-*exo*-anomeric conformations was detected in solution for the first time in naturally occurring sugars. This unusual behavior is attributed to branching. Here, polar contacts between non-vicinal sugar units lead to an enhanced flexibility of the ribose glycosidic torsion ϕ. The influence of sugar flexibility on RNA recognition will also be discussed.

Keywords: anomeric effect · antibiotics · molecular dynamics · molecular recognition · NMR spectroscopy

Introduction

Carbohydrates play a key role in energy storage and as constituents of the structural framework of cells and tissues. Due to their extraordinary capacity to encode information stereochemically, saccharides take part in a wide variety of recognition processes of biological significance. Thus, carbohydrate recognition by proteins has been shown to be involved in viral and microbial infection, plants defense, inflammatory responses, innate immunity, fertilization, tumor spread, and growth regulation.[1, 2] The three-dimensional structure of the oligosaccharides plays an essential role in their interaction with proteins and nucleic acids and thus determines their biological function. In this sense, a proper understanding of the different factors that govern sugar–protein/DNA/RNA interactions requires a detailed knowledge of the three-dimensional structure of the oligosaccharide in both the free and bound state. Although in most cases both conformations are basically identical this can not be considered a general rule and in recent years some cases of conformational selection by protein receptors have been reported.[3a–c] Consequently, the rigidity versus flexibility of natural oligosaccharides is an issue of great interest, because it concerns the potential adaptability of these ligands to the spatial and electronic requirements of the receptor. Although absolute rigidity can obviously be ruled out, the views concerning the degree of flexibility have evolved from the only very restricted fluctuations around a preferred conformations to a wide variability around the glycosidic linkages with different conformations in exchange depending on their nature. Thus, the presence of "*anti*-Ψ" and "*anti*-ϕ" conformations (Ψ/ϕ (H-C-O-C) = 180°) in solution for some particular linkages was first suggested by molecular mechanics calculations and later detected by NMR spectroscopical

[a] Dr. J. L. Asensio, A. Hidalgo, I. Cuesta, Dr. C. Vicent, Dr. J. L. Chiara
Instituto de Química Orgánica, CSIC
Juan de la Cierva 3, 28006 Madrid (Spain)
Fax: (+34)-91-5644853
E-mail: iqoa110@iqog.csic.es

[b] Dr. C. González
Instituto de Estructura de la Materia
CSIC, Madrid (Spain)

[c] Dr. J. Cañada, Prof. Dr. G. Cuevas, Prof. Dr. J. Jiménez-Barbero
Centro de Investigaciones Biológicas
CSIC, Madrid (Spain)

[d] Prof. Dr. G. Cuevas
On sabbatical leave, permanent address:
Instituto de Quimica
Universidad Nacional Autónoma de Mexico
Circuito exterior, Ciudad Universitaria
04510 Coyoacan, D.F. (Mexico)

Supporting information for this article (Figures showing details of the NMR analysis n and ribostamycin) is available on the WWW under http://www.chemeurj.org or from the author.

  0947-6539/02/0822-5228 $ 20.00+.50/0

methods.[4, 5] Nevertheless it has to be pointed out that in all cases these "*anti*" conformations were populated not higher than 5%. In addition, despite this conformational variability, all these major and minor conformers are in agreement with the *exo*-anomeric effect. In fact, not a single case of a non-*exo*-anomeric orientation around ϕ angle has ever been detected experimentally in solution for naturally occurring O-glycosides.

Aminoglycosides of the neomycin family are a class of clinically relevant antibiotics that bind to the decoding region aminoacyl-tRNA site (A-site) inducing codon misreading and inhibiting translocation.[6–7] From a chemical point of view they are cationic oligosaccharides characterized by the presence of a 4,5-disubstituted 2-deoxy-streptamine unit. The structure of paromomycin (an oligosaccharide of the neomycin family) in complex with its target RNA has been recently described.[7–9] According to the coordinates available from X-ray studies,[8–9] the structure of the sugar in the RNA-binding pocket can be described in terms of a single *exo*-anomeric conformation for the three glycosidic linkages. It has been suggested that this corresponds to the sugar conformation in solution and therefore the RNA recognises and binds "native" solution conformers of the drugs without inducing major structural distortions.[10] Here we show that, despite its branched nature, this antibiotic is very flexible and has a large percentage of non-*exo*-anomeric conformations in solution. Therefore, the molecular recognition process implies a conformational selection phenomenon. To the best of our knowledge this antibiotic represents the first reported case of occurrence of a large population on non-*exo*-anomeric conformers in solution for an O-glycoside.

Results and Discussion

Structural analysis of neomycin B in solution

In order to determine the influence of the protonation on the conformational preferences of neomycin B the structural analysis was carried out at two different pH values namely 4.7 and 9.7 corresponding to the fully protonated and neutral states, respectively.

pH 4.7 (fully protonated state): As a first step, selective one-dimensional NOE experiments were carried out at 313 K and pH 4.7. The branched nature of neomycin B (Figure 1a) allowed the measurement of an unusually large number of structurally relevant NOE values (Figures 1, 2 and S1, Supporting Information). In addition, ^3J values were measured for the ribose ring (Table 1). The analysis of the coupling constants for the idose ring show unambiguously that the $^1C_4$(L) conformer (with three axial and two equatorial

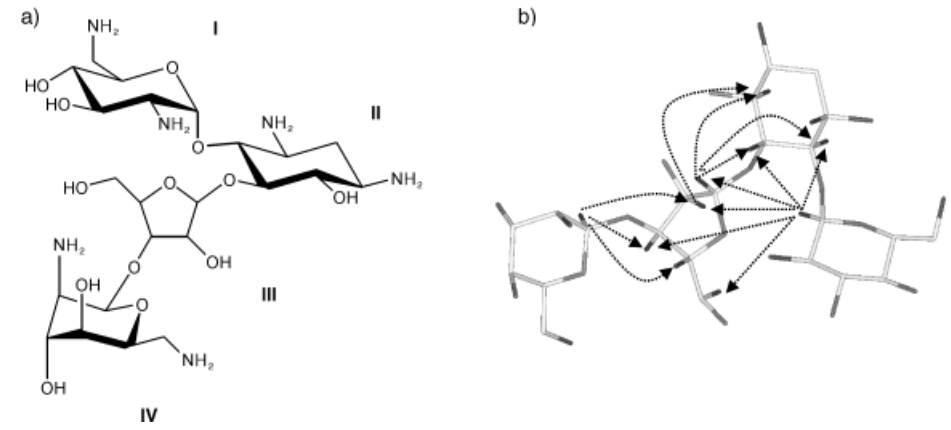

Figure 1. a) Schematic representation of neomycin B along with the numbering employed for the different sugar units. b) Structurally relevant interproton distances measured in neomycin B at 313 K and pH 4.7.

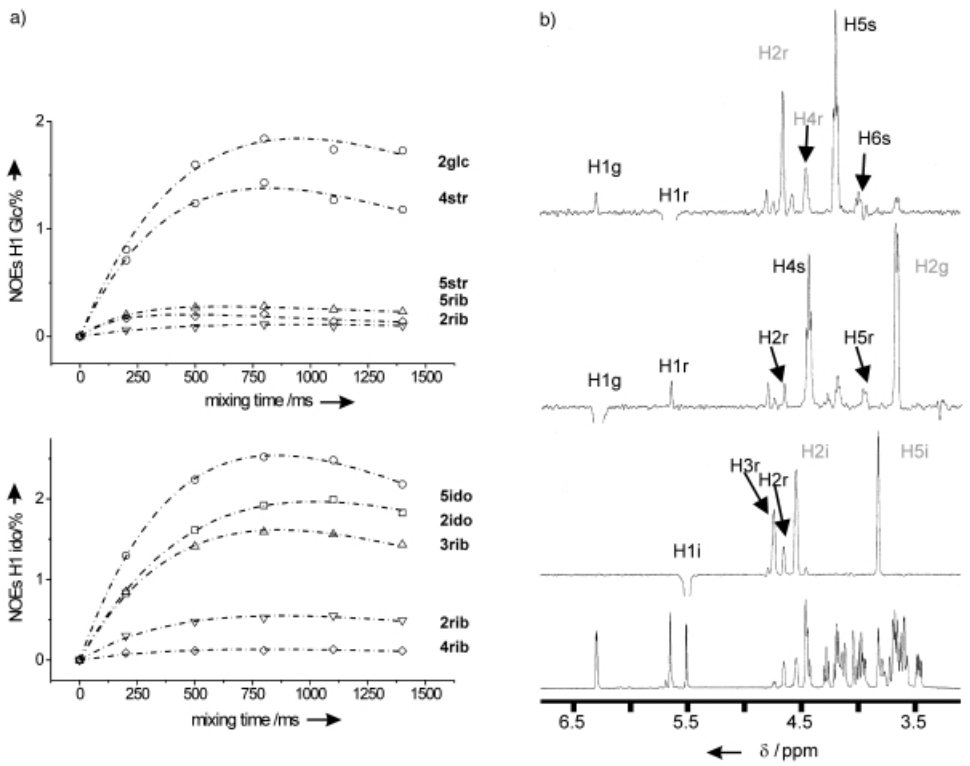

Figure 2. a) Experimental build-up curves obtained from selective 1D NOE experiments with the 1D-DPFGSE NOE pulse sequence at 5 mixing times, 313 K and pH 4.7 for neomycin B. b) Selective 1D NOE experiments with the 1D-DPFGSE NOE pulse sequence, corresponding to the inversion of $H1_{Rib}$, $H1_{Glc}$ and $H1_{Ido}$(from top to bottom).

  0947-6539/02/0822-5229 $ 20.00+.50/0

Table 1. Experimental and theoretical distances and coupling constant values obtained for aminoglycosides of the neomycin family.[a]

	Neomycin B pH 4.5				Neomycin B pH 9.7		Ribostamycin pH 4.5		Neamine pH 4.5	
d [Å]	Exptl	MD PBC [10 ns]	MD-tar J PBC [1 ns]	MD-tar [80 ns]	Exptl	MD-tar [80 ns]	Exptl	MD-tar [80 ns]	Exptl	MD-tar [80 ns]
$H1_{Glc}-H4_{Strp}$	2.5	2.7	2.8	2.6	2.5	2.5	2.5	2.7	2.4	2.5
$H1_{Glc}-H5_{Strp}$	3.0	3.0	2.9	3.1	>3.5	3.4	3.1	3.1	3.6	3.5
$H1_{Glc}-H3_{Strp}$	–	–	–	–	3.4	3.2	–	–	>4.0	4.2
$H1_{Glc}-H5_{Rib}$	3.0	3.2	4.5	3.1	–	–	3.3	3.4	–	–
$H1_{Glc}-H2_{Rib}$	3.6	3.1	3.1	3.4	3.6	3.4	3.6	3.3	–	–
$H1_{Glc}-H3_{Rib}$	>3.5	3.6	3.2	3.1	>3.5	3.5	>3.5	3.1	–	–
$H1_{Rib}-H5_{Strp}$	2.3	2.5	2.6	2.5	2.3	2.6	2.2	2.5	–	–
$H1_{Rib}-H4_{Strp}$	>4.0	4.5	>4.0	4.4	2.7	2.9	>3.5	3.7	–	–
$H1_{Rib}-H6_{Strp}$	3.6	3.3	3.2	3.3	3.1	3.0	3.3	3.1	–	–
$H2_{Rib}-H6_{Strp}$	3.3	3.3	3.3	3.4	3.8	3.6	3.1	3.2	–	–
$H1_{Rib}-H4_{Rib}$	3.2	3.1	3.1	3.1	3.2	3.1	3.1	3.2	–	–
$H1_{Ido}-H3_{Rib}$	2.6	2.7	2.7	2.5	2.4	2.5	–	–	–	–
$H1_{Ido}-H2_{Rib}$	3.1	3.0	2.7	3.0	2.6	2.7	–	–	–	–
$H1_{Ido}-H4_{Rib}$	3.9	4.1	4.3	3.7	>4	4.0	–	–	–	–
J [Hz]	Exptl	MD PBC [10 ns]	MD-tar J PBC [1 ns]	MD-tar [80 ns]	Exptl	MD-tar [80 ns]	Exptl	MD-tar [80 ns]	Exptl	MD-tar [80 ns]
$H1_{Rib}-H2_{Rib}$	2.7	4.3	3.2	3.2	2.7	2.7	2.0	2.6	–	–
$H2_{Rib}-H3_{Rib}$	4.5	4.0	4.3	4.0	4.5	4.6	4.5	4.0	–	–
$H3_{Rib}-H4_{Rib}$	6.3	4.6	6.1	5.8	6.4	6.3	6.8	6.4	–	–
$H4_{Rib}-H5r_{Rib}$	5.5	4.5	2.1	5.2	4.5	4.2	5.8	6.1	–	–
$H4_{Rib}-H5s_{Rib}$	3.2	3.2	2.8	3.8	2.7	2.6	2.9	3.8	–	–

[a] For neomycin B at pH 4.7 average distances and J values obtained from unrestrained MD simulations, from MD-tar runs including only J information, and from MD-tar simulations using coupling constants and distances are shown for comparison. Unrestrained simulations and MD-tar runs including only J values were carried out using explicit solvent, periodic boundary conditions (PBC), and Ewald sums for the treatment of electrostatic interactions (see the experimental part). In vacuo MD-tar runs were run with $\varepsilon = 80$.

substituents) is the major conformer in water($>98\,\%$). All ^{1}H NMR signals for the idose H1 – H4 ring protons are broad singlets, which is in agreement with a *gauche*-type arrangement of the vicinal proton pairs. In addition, a very strong H-1/H-5 intraresidue NOE indicates a *syn*-diaxial relationship for this proton pair.

Careful inspection of all the NOE and J data immediately suggest the existence of a significant degree of internal mobility in the tetrasaccharide, because no single structure can satisfy all the constraints simultaneously. In order to obtain an experimentally derived ensemble, 80 ns MD-tar[11] simulations (in vacuo, $\varepsilon = 80$) were carried out by including five coupling constants (see Table 1) and 14 experimental distances as time-average restraints with the AMBER 5.0 program.[12] In addition, 10 ns unrestrained MD simulations were performed for comparison. The obtained MD-tar distribution of conformers for every particular glycosidic linkage is shown in Figure 3a, superimposed on the MM3* steric maps previously calculated. It can be observed that for the Glc α(1-5)2-deoxy-Strp linkage a major population is centered around $\phi/\psi = -45^\circ/-45^\circ$. A minor population around $\phi/\Psi = -25^\circ/30^\circ$ was also detected. In contrast, the Ido β(1-3)Rib linkage is characterized by a high degree of flexibility with two different conformations almost equally populated located at $\phi/\Psi = -50^\circ/-40^\circ$ and $\phi/\Psi = -50^\circ/40^\circ$. Nevertheless, both glycosidic linkages exhibit common features: ϕ values are scattered around the *exo*-anomeric region; the conformational flexibility is mainly restricted to the aglyconic ψ torsion. This constitutes the usual behavior in all naturally occurring O-glycosides described thus far. A totally different behavior is observed for the Rib β(1-6)2-deoxy-Strp linkage. In this case, two populations characterized by different ϕ values ($50^\circ/25^\circ$ and $-10^\circ/25^\circ$) were detected. In contrast to common behavior, this glycosidic linkage shows a larger degree of mobility around ϕ than around ψ. Moreover, MD-tar simulations indicate that a large percentage of the population ($>30\,\%$) is located in non-*exo*-anomeric regions with ϕ about -10°. Indeed, the occurrence of a non-*exo*-anomeric orientation around ϕ_{Rib} is experimentally proven by a medium NOE $H2_{Rib}$-$H6_{Strp}$, exclusive of this conformational region. That is, the existence of a short $H\text{-}2_{Rib}/H\text{-}6_{Strp}$ average distance can never be explained without assuming a remarkable deviation from the *exo*-anomeric region for ϕ_{Rib} (the $H\text{-}2_{Rib}/H\text{-}6_{Strp}$ distance for the *exo*-anomeric region is longer than 4.1 Å).

Sensitivity of the results to the simulation conditions: Is important to bear in mind that, despite the relatively large number of experimental constraints employed (twice or three times the usual number), the system has still a certain degree of underdetermination. This is a normal problem when flexibility is considered for the interpretation of NMR data of biomolecules in general, and of carbohydrates in particular. Thus, in principle, some dependency of the different conformational populations on the computational details would be expected. However, this dependency can in principle be assessed by performing the MD simulations under a variety of different conditions and protocols. Thus, for neomycin B, additional MD simulations were carried out (Figure 4, S2): Unrestrained; including only J information as time-averaged constraints, (Thus, we warranted that the ribose puckering

  0947-6539/02/0822-5230 $ 20.00+.50/0 *Chem. Eur. J.* **2002**, *8*, No. 22

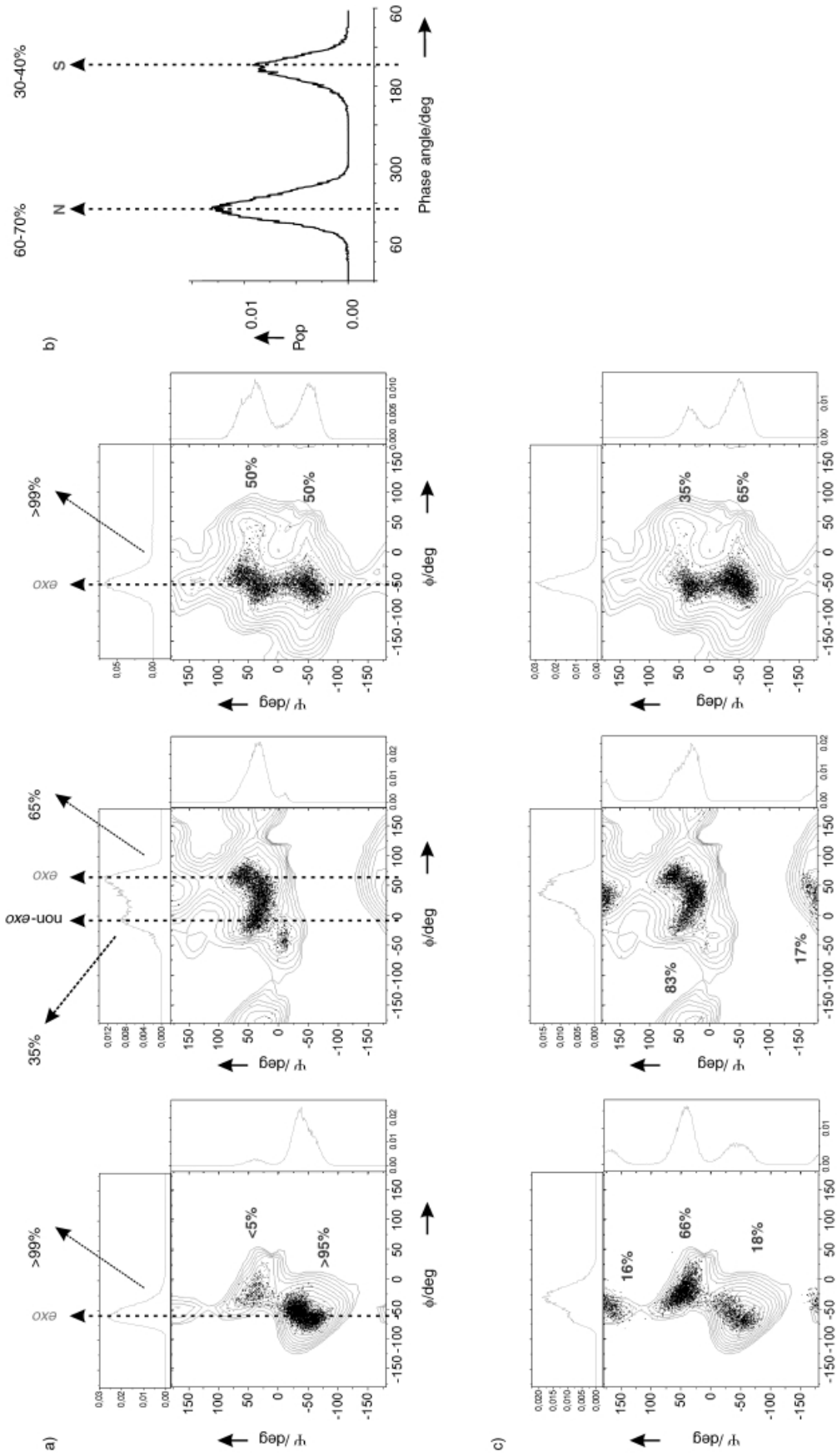

Figure 3. a) Experimentally derived MD-tar distributions obtained from a 80ns length simulation for the Glc/Strp (left), Strp/Rib (middle) and Rib/Ido (right) linkages at pH 4.7(the fully protonated state). The presence of a very significant non-*exo*-anomeric population for the Strp/Rib linkage (middle) is highlighted in black. Bottom: Ribose puckering distribution from MD-tar simulations is also shown. b) Experimentally derived MD-tar distributions obtained from a 80 ns length simulation for the Glc/Strp (left), Strp/Rib (middle) and Rib/Ido (right) linkages at pH 9.7 (the neutral state).

  0947-6539/02/0822-5231 $ 20.00+.50/0

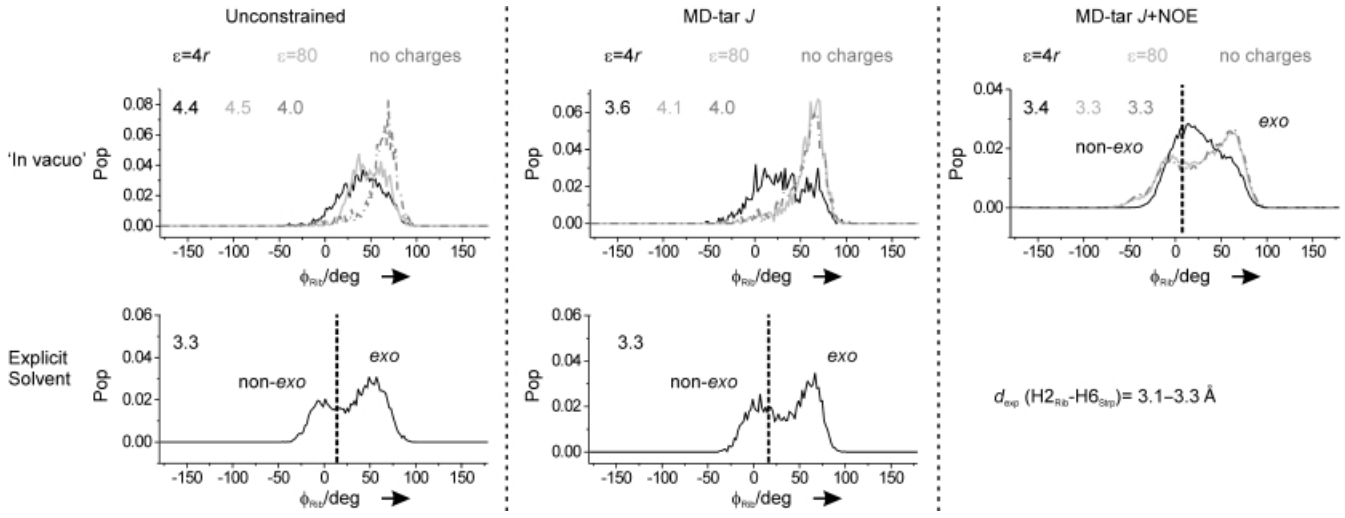

Figure 4. ϕ_{Rib} distributions obtained from MD simulations carried out for neomycin B under a variety of different conditions (from left to right, unconstrained, including only *J* or both *J* and NOE values). In all cases the theoretical key distance $H2_{Rib}-H6_{Strp}$ is indicated. The experimental value is shown in the right-hand corner.

distribution is reproduced by the calculations) including both *J* and NOE information, as time-averaged restraints.

In addition, different conditions were tested for both restrained and unrestrained simulations. Thus, calculations were run: without charges; with charges and $\varepsilon = 80$; with charges and $\varepsilon = 4r$; with charges, explicit solvent, periodic boundary conditions, counterions, and Ewald sums for the treatment of the electrostatic interactions.

Finally, for the constrained trajectories, different simulation lengths, force constants, and exponential decay coefficients were also tested. In all cases, average distances and *J* values were calculated and compared with the experimental ones. The obtained results can be summarized as follows:

- As expected for a charged molecule such as neomycin B, the results of the simulations are sensitive to the computational details in absence of experimental constraints (Figure 4). Thus, depending on the conditions a rather different behavior for the ribose moiety is observed. Although, none of this calculations were able to fully reproduce the experimental data, the best results were clearly obtained when explicit solvent (TIP3P water), periodic boundary conditions, counterions and Ewald sums for the treatment of the electrostatic interactions were employed (see Table 1). In this case, a qualitative agreement between theoretical and experimental *J* and NOE data was obtained. This trajectory was the only unrestrained one able to reproduce the non-*exo*-anomeric NOE $H2_{Rib}$-$H6_{Strp}$.
- MD-tar trajectories including only *J* information were also found to be sensitive to the simulation conditions (Figure 4). Although the ribose puckering distribution was correctly reproduced, large violations of the experimental distances were observed in all cases for the "in vacuo" runs (independently of the dielectric constant). In contrast, a reasonable agreement between theoretical and experimental data was obtained when explicit solvent and counterions were included in the calculation. Once again, this trajectory was the only one able to reproduce the non-*exo*-anomeric NOE $H2_{Rib}$-$H6_{Strp}$.
- MD-tar simulations including both NOE and *J* information were found to correctly reproduce the experimental data *independently* of the simulation conditions. More important, the conformational behavior predicted for neomycin B was very similar in all cases. Although some differences in the obtained distributions for ϕ_{Rib} can be observed (Figure 4) in all cases, the calculations predicted the existence of remarkable deviations from the *exo*-anomeric region for this glycosidic torsion. Interestingly, simulations carried out with explicit solvent (both unrestrained or including only *J* restraints) predicted very similar non-*exo*-anomeric populations for ϕ_{Rib} than those reproduced by the "in vacuo" trajectories that included both NOE and *J* information.

Lastly, it has to be mentioned that potential energy curves for the rotation around ϕ_{Rib} were also obtained employing both the MM2* and MM3* force-fields (Figure S3, Supporting Information). In all cases the calculations predict the existence of an enhanced flexibility for this glycosidic torsion together with significant deviations from the normal *exo*-anomeric region.

Comparison of all these data clearly indicate that a correct puckering distribution for the ribose ring together with a significant non-*exo*-anomeric (between 10° and -30°) population for ϕ_{Rib} (between 20% and 30% depending on the conditions) are indeed essential in order satisfy the $H2_{Rib}-H6_{Strp}$ NOE. This conclusion is not based on the analysis of a single MD trajectory, but on the extensive comparison of the results obtained under many different simulation conditions. In this sense, our results are relatively independent of the particular computational details (force field, charges etc.) of the calculations.

Ribose conformation and neomycin structure: Interestingly, there is a strong correlation between the Rib ring conformation and the glycosidic torsion ϕ_{Rib} according to the MD-tar. The experimentally derived puckering distributions (Fig-

0947-6539/02/0822-5232 $ 20.00+.50/0 *Chem. Eur. J.* **2002**, *8*, No. 22

ure 3a) show the presence of two different conformational regions populated in solution with phase angles around 20° (60–70%) and 160° (30–40%) (herein referred as "N" and "S" regions, respectively). Thus, when the Rib ring is in the "S" state, ϕ adopts values for the *exo*-anomeric region (Figure 5). In contrast, for the "N" region, ϕ presents significant deviations from the *exo*-anomeric values. This behavior is reproduced by MD-tar simulations carried out including only the *J* values for the ribose unit as restraints. To provide an explanation for this observation MD simulations of neomycin B were run both "in vacuo" ,with $\varepsilon = 1$ and $\varepsilon = 80$, and with explicit solvent (see the Experimental Section). Ribose puckering was switched from "N" to "S" state by means of dihedral angle constraints and the effect on ϕ_{Rib} was monitored. Figure 6a shows the observed variations in ϕ_{Rib}. In the first half of the MD-run, the ribose puckering is "N", while it adopts the "S" state during the second half. With $\varepsilon = 1$, significant deviations from the *exo*-anomeric regions were observed for both sugar puckerings. Detailed inspection of the structures shows the presence of a bifurcated hydrogen bond involving the amino group at position 2 of the glucose unit as a donor and both O4 and O5 in the ribose as acceptors (Figure 6b). This polar contact between the non-vicinal residues is responsible for the observed shift in ϕ_{Rib} towards non-*exo*-anomeric regions. In fact, for the "in vacuo" runs with $\varepsilon = 80$, all glycosidic torsions are in agreement with the *exo*-anomeric effect independent of the ribose ring conformation. MD-runs in presence of explicit water molecules and counterions (see the Experimental Section) indicates that the polar contacts between the non-vicinal Glc and Rib units are selectively disrupted by solvent only for the "S" puckering, but not for the "N" (Figure 6). Thus, the different effect of the solvent on both species are at the origin of the observed correlation between the ribose ϕ angle and the sugar conformation. As a final test, solvated MD-tar simulations of the non-branched 2,6-dideoxy-2,6-diamino-L-Ido-β(1-3)-Rib-β(1-5)-2-deoxy-Strp fragment of neomycin B (rings II, III and IV) were carried out employing only theoretical *J* restraints for the ribose. The results obtained for this linear trisaccharide conclusively show that in absence of branching the overall rigidity around ϕ_{Rib} increases, independently of the puckering distribution considered for the ribose, and now all torsion values are consistent with the *exo*-anomeric effect (Figure 7). It has to be mentioned that the conformational behavior of the Rib/Strp linkage in neomycin B is qualitatively reproduced (see Table 1) by this kind of MD-runs (including only experimental *J* information for the ribose ring).

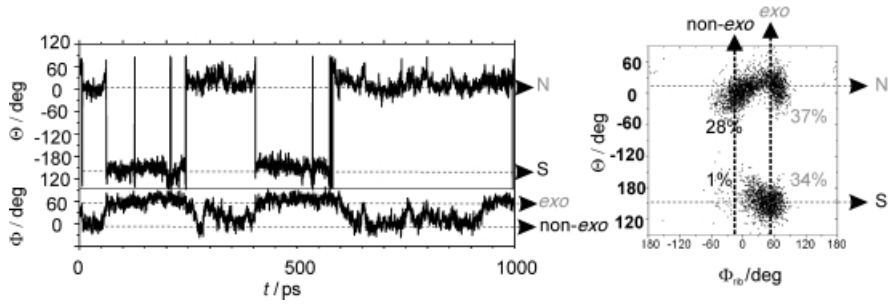

Figure 5. Left: Variations in ϕ_{Rib} (bottom) and the Rib puckering phase angle (top) during a few picoseconds of the MD-tar simulations. Deviations from the *exo*-anomeric region are strongly correlated with the ring puckering. Right: Representation of the phase angle (Θ) vs glycosidic torsion angle (ϕ) for the ribose unit. It can be observed that non-*exo*-anomeric ϕ_{rib} orientations are significantly populated only for a "N" puckering.

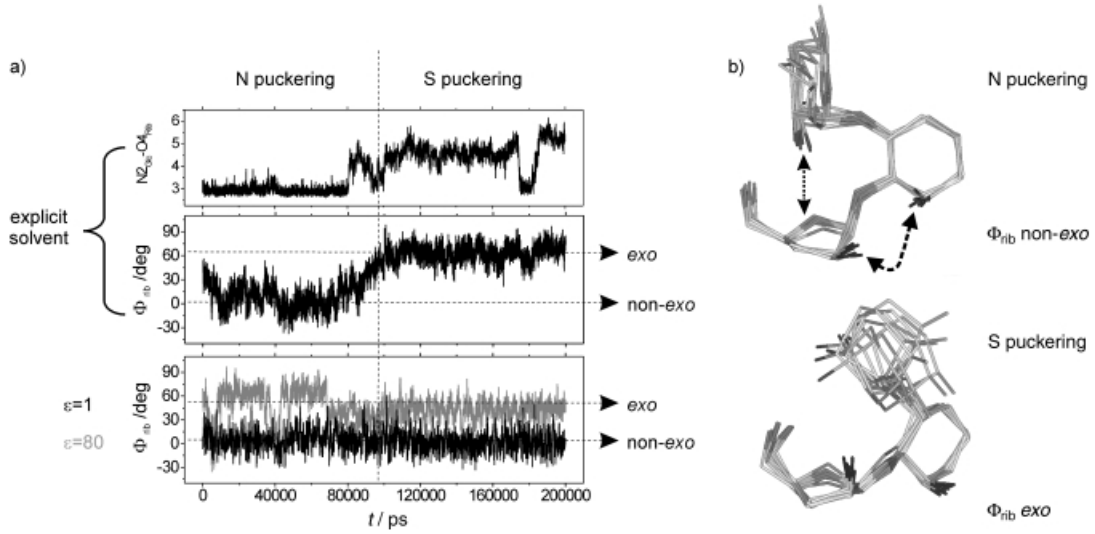

Figure 6. a) Schematic representation of the observed variations in ϕ_{Rib} during 1 ns of a "in vacuo" MD simulation with $\varepsilon = 1$ and $\varepsilon = 80$ (bottom) and a solvated MD simulation with explicit solvent, periodic boundary conditions and Ewald sums for the treatment of electrostatic interactions (middle). In all cases, ribose puckering was switched from "N" to "S", in the middle of the simulation, employing dihedral angle constraints and its influence on ϕ_{Rib} was monitored. Variations in the distance between amino group at position 2 of the glucose and $O4_{Rib}$ during the solvated MD run are represented in the upper part of the figure. b) Snapshots, taken from the solvated MD simulation, corresponding to neomycin B with the Ribose in the "N" (upper part) and "S" (lower part) states. Polar contacts between the non-vicinal Glc and Rib moieties are shown in the upper part. In addition, the $H2_{Rib}$–$H6_{Strp}$ NOE, characteristic of non-*exo*-anomeric ϕ_{Rib} angles is shown for the "N" puckering (uppert part).

In a similar way, the conformational properties of the Ido/Rib linkage seem to be correlated with the ribose structure (Figure 8). Thus, ψ angle adopts mainly positive values (around $+45^\circ$) for a "S" ribose and negative (around -50°) for a "N" conformation (although it is significantly more flexible for the later case). It is well known that conformational preferences around ψ angle in natural O-glycosides are modulated by 1:3 *syn*-diaxial interactions[13] with vicinal OH groups (Figure 8). Accordingly, conformational populations characterized by negative ψ values (Figure 3a) would be destabilized by a 1:3-type contact with the pseudoequatorial $OH2_{rib}$ only for the "S" puckering (Figure 8). This contact does not exist for a ribose "N" conformation where $OH2_{rib}$ is pseudoaxial and therefore a larger flexibility is expected, also in agreement with the MD-tar results.

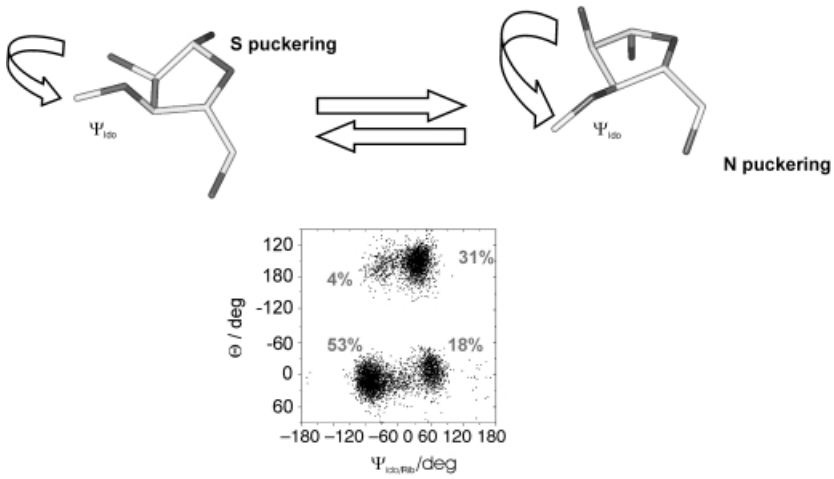

Figure 8. Top: 1,3-*syn*-diaxial interactions established by $OH2_{Rib}$ and $OH5_{Rib}$ with the vicinal $OH3_{Rib}$ group are dependent on the ribose ring conformation. Bottom: Schematic representation of the ribose phase angle (Θ) vs ψ_{Ido} from a 80 ns MD-tar simulation including both distance and J values. Both parameters are strongly correlated. Thus, ψ_{Ido} adopts positive values mainly for the "N" ribose puckering. This orientation is destabilized for the "S" ribose puckering by a 1,3-*syn*-diaxial interaction with the pseudoequatorial $OH2_{Rib}$ group.

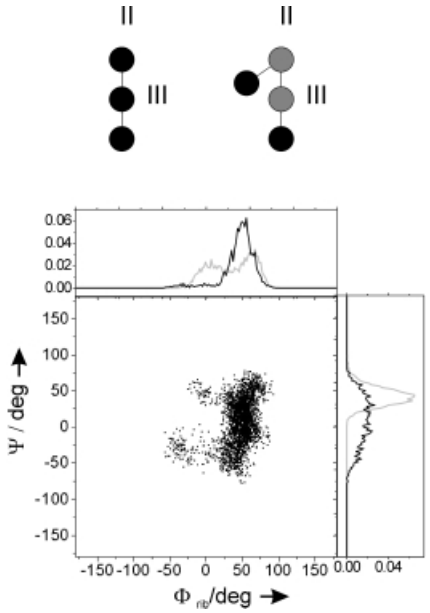

Figure 7. ϕ_{Rib} and ψ_{Rib} distributions for the non-branched 2,6-dideoxy-2,6-diamino-L-Ido-β(1-3)-Rib-β(1-5)-2-deoxy-Strp fragment of neomycin B (rings II, III and IV), obtained by solvated MD-tar simulations employing only theoretical J constraints. Interestingly, the conformational behavior of the Rib/Strp linkage in neomycin B is qualitatively reproduced (see Table 1) by this kind of MD-runs (including only experimental J information for the ribose ring). Surprisingly, comparison between MD runs for both compounds conclusively show that the overall rigidity around ϕ_{Rib} increases in the non-branched trisaccharide with respect to the tetrasaccharide, independently of the puckering distribution considered for the ribose in the former case. In fact for the linear trisaccharide, all torsion values are consistent with the *exo*-anomeric effect. ϕ_{Rib} and ψ_{Rib} distributions for the trisaccharide are shown in black. The corresponding distributions for the whole tetrasaccharide are shown in grey for comparison.

Experimental evidence of neomycin B flexibility: According to the MD-tar simulations the Ido/Rib linkage has the larger degree of internal mobility in the tetrasaccharide followed by the Rib/Strp bond. This point is further supported by the dependency exhibited by the intraresidue NOEs on temperature for the different sugar units. Figure 9 shows selective

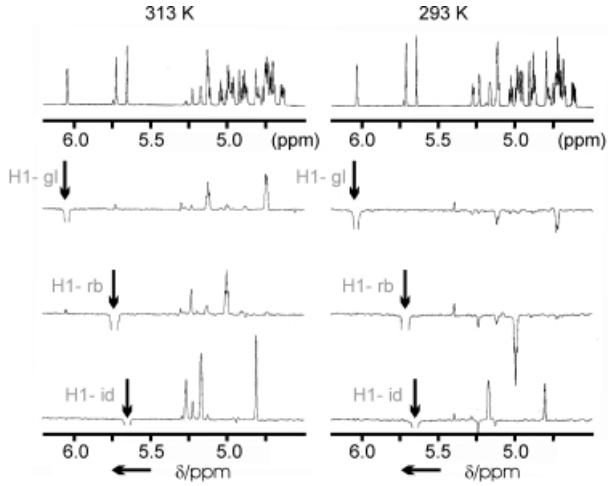

Figure 9. Dependency exhibited by the intraresidue NOEs on temperature for the different sugar units. Selective NOEs obtained upon inversion of the three anomeric protons at 313 K (left) and 293 K (right). It can be observed that at 313 K the three sugar units (Glc, Rib and Ido) present positive NOEs. In contrast, at 293 K an inversion in the sign of the intraresidue contacts is observed for the Glc and Rib units but not for the Ido ring.

NOEs obtained upon inversion of the three anomeric protons at 313 K (left) and 293 K (right). It can be observed that, at 313 K, the three sugar units (Glc, Rib and Ido) present positive NOEs (high mobility). In contrast, at 293 K, an inversion in the sign of the intraresidue contacts is observed for the Glc and Rib units but not for the Ido ring. This observation is consistent with a shorter local correlation time for this terminal residue. The ribose unit also exhibits a large

0947-6539/02/0822-5234 $ 20.00+.50/0 *Chem. Eur. J.* **2002**, *8*, No. 22

degree of flexibility according to the MD-tar data. However, in this case, internal mobility around the glycosidic linkage is couple to the "N"/"S" exchange in the furanose ring and influenced by remote contacts with the Glc sugar moiety. Therefore a larger energy barrier and a slower conformational exchange would be expected.

pH 9.7 (the neutral state): In a second step, the structural analysis of the oligosaccharide was carried out at pH 9.7, corresponding to the neutral state of the molecule. First, *J* values for the Rib and Ido rings were found to be identical to that observed at acidic pH values. However, qualitative inspection of the structurally relevant NOE values indicates the existence of significant conformational differences between the neutral species and the fully protonated neomycin B. First, a shorter $H1_{Glc}-H3_{Strp}$ average distance is deduced for Glc/Strp linkage (see Table 1). This is consistent with an increase in the population around $\phi/\Psi=-40°/180°$ region (*anti* ψ region). In a similar way, a very significant shortening in the $H1_{Rib}-H4_{Strp}$ and $H1_{Rib}-H6_{Strp}$ is observed for the Rib/Strp linkage probing the presence in solution of a certain population around $\phi/\Psi=50°/180°$ (*anti* Ψ minima). In addition, an increase in the average $H2_{Rib}-H6_{Strp}$ indicates that, under these conditions, the deviations of ϕ_{Rib} from the *exo*-anomeric region are less pronounced that those observed at pH 4.7. This observation strongly suggests that the polar interactions between the Glc and Rib units, previously described, are weaker in the neutral antibiotic. Finally, the shortening of the average $H1_{Ido}-H2_{Rib}$ distance suggests a slightly different conformational behavior for this linkage. In order to get an experimentally derived ensemble, 80 ns MD-tar simulations ("in vacuo", $\varepsilon=80$) were carried out by including five *J* coupling constants (see Table 1) and 13 experimental distances as time-average restraints. The obtained MD-tar distribution of conformers for every particular glycosidic linkage is shown in Figure 3 b, superimposed on the steric MM3* maps. As expected, a much larger degree of flexibility is observed in neutral neomycin B with respect to the fully charged antibiotic. Significant differences between both pH values are evident for the three glycosidic linkages. First, at basic pH, for the Glc-Stpr fragment there is an increase in the population around $\phi/\Psi \approx -20°/40°$. In addition, a minor *anti*-ψ ($\phi/\Psi=-40°/180°$) population is also detected. Similarly, the Rib/Strp linkage shows a large mobility around ψ with a significant percentage of *anti*-ψ conformation (50°/180°). Additionally, non-*exo*-anomeric orientations around ϕ_{Rib} are clealy reduced with respect to the low pH studies. Finally, for the Ido/Rib linkage a shift in population from minimum $\phi/\Psi=-50°/40°$ to $\phi/\Psi=-50°/-40°$ takes place.

Structural analysis of ribostamycin and neamine in solution

The NMR analysis of the neomycin B fragments ribostamycin and neamine was also carried out for comparison purposes. Experimentally derived distances and *J* values at pH 4.7 are shown in Table 1. For ribostamycin, their comparison with those previously obtained for the whole tetrasaccharide (see Table 1) suggests that the structural differences between them are almost negligible. In fact, a clear $H2_{Rib}-H6_{Strp}$ NOE characteristic of non-*exo*-anomeric populations around ϕ_{Rib} was also observed for the trisaccharide (Figure 10). The MD-tar simulations indicate that the conformational behavior of ribostamycin is almost identical with that previously described for neomycin B. The obtained MD-tar distribution of conformers for every particular glycosidic linkage in ribostamycin is shown in Figure S4 in the Supporting Information.

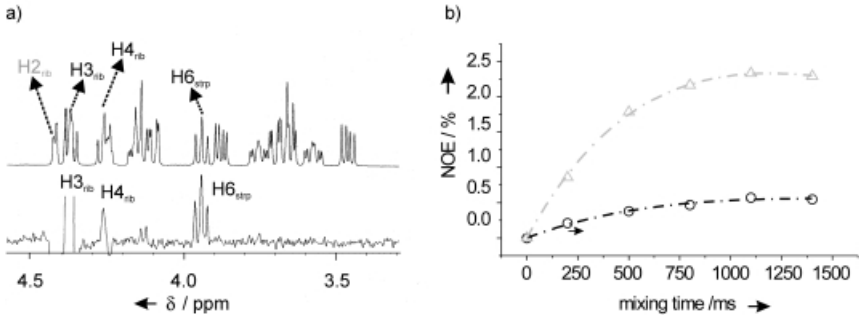

Figure 10. a) Selective 1D NOE experiment with the 1D-DPFGSE NOE pulse sequence, corresponding to the inversion of $H2_{Rib}$, in ribostamycin at pH 4.7. The $H2_{Rib}-H6_{Stpr}$ characteristic of non-*exo*-anomeric ϕ_{Rib} populations is shown. b) Experimental build-up curves corresponding to the interresidue $H6_{Strp}-H2_{Rib}$ and the intraresidue $H6_{Strp}-H4_{Strp}$ NOEs obtained from selective 1D NOE experiments with the 1D-DPFGSE NOE pulse sequence at five mixing times, 313 K and pH 4.7.

In a similar way, NMR analysis of neamine indicates the existence of slight structural differences with respect to the Glc/Strp fragment in the tetrasaccharide. Thus, ϕ angle is slightly shifted towards lower values (40°, Figure 11). Furthermore a different population of rotamers around ψ is observed (Figure 11) in the disaccharide. These differences are the result of remote contacts between the Glc/Rib units in neomycin B, which are obviously absent in neamine.

Summary and discussion of the results obtained for the antibiotics in the free state

Several conclusions can be drawn from these results. First, structural analysis of neomycin B and ribostamycin in the free state unequivocally shows that flexibility in natural O-glycosides is not restricted to the aglyconic ψ angle, but in certain cases ϕ can also undergo conformational fluctuations, even adopting non-*exo*-anomeric orientations. To the best of our knowledge these antibiotics represent the first reported case of occurrence of a large population of non-*exo*-anomeric conformers in solution. Here, this unusual behavior has its origin in the presence of polar and steric contacts between the non-vicinal glucose and ribose moieties.

  0947-6539/02/0822-5235 $ 20.00+.50/0

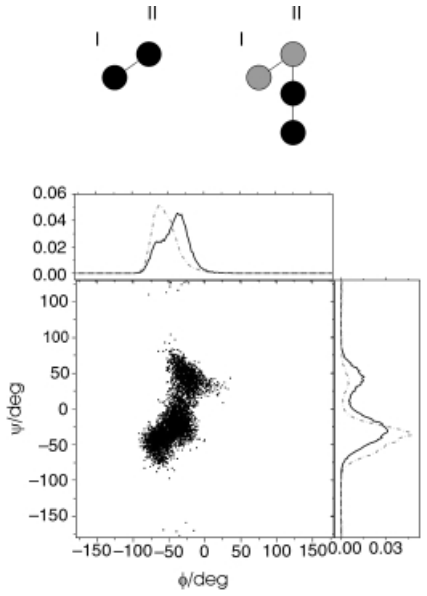

Figure 11. ϕ_{Rib} and ψ_{Rib} distributions for the disaccharide (——) Neamine obtained by solvated MD-tar simulations employing experimental distance and J constraints (see Table 1). The experimentally derived ϕ_{Rib} and ψ_{Rib} distributions for this neomycin fragment in the tetrasaccharide are shown for comparison (----).

In order to estimate the energy cost for the observed ϕ_{Rib} deviations from the *exo*-anomeric region, calculations at B3LYP/6-31G(d,p) level of theory for both ribose sugar puckers were carried out employing the model shown in Figure 12.[14] Potential energy curves corresponding to ϕ variations between 120° and −60° were obtained by restrained geometry optimization. Two different minima (A and

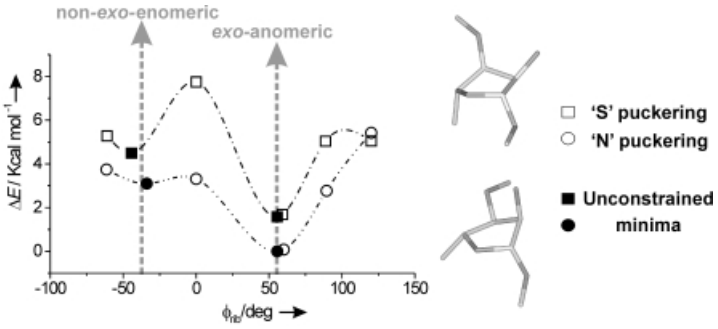

Figure 12. Potential energy curves corresponding to ϕ variations between 120° and −60° obtained by restrained geometry optimization at the B3LYP/6-31G(d,p) level of theory for both ribose sugar puckers. Minima were identified by full geometry optimization.

B, Figure 12) were identified for both sugar puckers by full geometry optimization. It can be observed that transition from minimum A (in the *exo*-anomeric region) to minimum B (non-*exo*-anomeric) has and energy cost of at least 2.9 kcal mol^{-1}. In contrast, as described above for the fully protonated state of neomycin B, this ΔG cost is 0.16 kcal mol^{-1} and 2.1 kcal mol^{-1} for the "N" and "S" puckerings, respectively, according to the MD-tar derived populations (Figure 5). As previously mentioned, polar and steric contacts between the non-vicinal Glc and Rib moieties, sensitive to ribose ring pucker, account for this relative stabilization of non-*exo*-anomeric conformations in neomycin B.

Many relevant saccharides, such as the blood group antigens, include sugar units glycosidated in contiguous positions. It has been assumed that this pattern of substitution increases overall rigidity of the ligand due to steric contacts between both substituents.[15] Our results indicate that this can not be considered a general rule and that this depends on the configuration and chemical nature of the contiguous sugar units. In neomycin-like antibiotics, rigidification of ψ_{Rib} angle is compensated by remarkable enhancement of the internal mobility around ϕ_{Rib}.

Structure and flexibility of neomycin-like antibiotics bound to A-site ribosomal RNA—Comparison with the free state

Carbohydrate mobility has been shown to play an important role in their recognition by proteins.[16] Thus, in some cases, sugar rigidification upon binding is known to make a significant contribution to the entropic barrier of the process. This effect has been suggested to be at the origin of the enthalpy/entropy compensation phenomenon usually observed for this kind of interactions.[16] Nevertheless, up to now, no detailed studies on the role of carbohydrate flexibility in their recognition by RNA have been reported. A proper understanding of the driving forces behind neomycin B recognition by its target RNA requires a detailed knowledge of the structure and dynamical behavior of the ligand in both the free and bound states. Our data provide a quantitative description of the neomycin B conformational behavior in solution and shows that, despite its branched nature, it is characterized by a remarkable flexibility with different conformations (even non-*exo*-anomeric ones) in fast exchange. If the oligosaccharide internal mobility is severely restricted upon binding to RNA then a significant entropic contribution to the global ΔG of the process would be expected. In fact, it has been suggested that the ligand rigidification could have a significant contribution to the global ΔS in aminoglycosides.[17] Both NMR[7] and X-ray[8, 9] studies provide detailed information about the three-dimensional structure of neomycin-like oligosaccharides in complexes with RNA. Thus, the structure of paromomycin (a tetrasaccharide of the neomycin family) in a complex with its target RNA has been described by both X-ray[8, 9] and NMR[7] methods in few years. These studies have provided a very detailed information on the conformational preferences of antibiotics of the neomycin family, bound to their target RNA.

In order to estimate the degree of conformational restriction imposed on neomycin B by the A-site RNA binding pocket, we carried out solvated MD simulations of the complex. Initial structures of the neomycin B/RNA complex were built from those reported for the paromomycin/A-site complex derived by both X-ray (pdb accession code 1FJG) and NMR methods (pdb accession code 1PBR). An independent 5 ns simulation was run from both starting coordinates. They were performed using periodic boundary conditions and the particle-mesh Ewald approach[18] to introduce long-range electrostatic effects. In all cases, RNA structures

0947-6539/02/0822-5236 $ 20.00+.50/0 *Chem. Eur. J.* **2002**, *8*, No. 22

were represented using AMBER-95 force-field parameters,[12] while water was represented by means of the TIP3P[19] model.

Figure 13 shows the all atom RMSD deviations observed during the 5 ns MD simulations with respect to the initial (experimental) structures. In both cases, the two terminal base pairs at each end of the RNA fragment and the flipped out residues A1492 and A1493 were excluded from the RMSD calculation. It can be observed that after a 5 ns run deviations from the X-ray experimental coordinates are below 1.2 Å. By contrast, this value is 3.2 Å for the trajectory that employed the NMR coordinates as starting point. Probably, the poorer definition of the RNA phosphate backbone in the initial NMR complex is responsible for this deviation. It has to be mentioned that all the stabilizing sugar/RNA contacts observed in the X-ray structure, and most of those reported for the NMR complex are preserved during the whole trajectories.

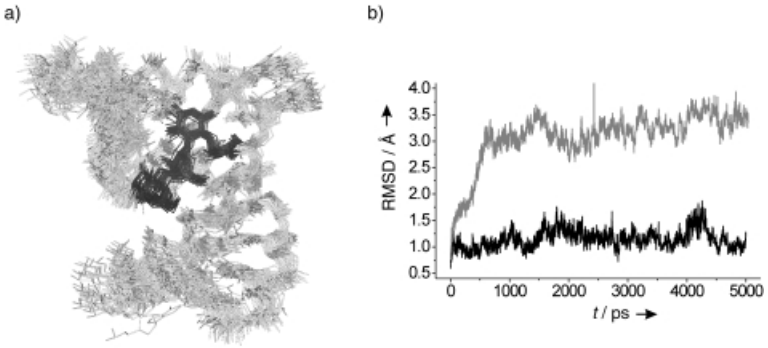

Figure 13. a) Snapshots taken from 5 ns MD simulations of to the neomycin B/A-site complex. The initial structure was built from the coordinates corresponding to the X-ray structure of the 30S ribosome subunit in complex with paromomycin (pdb accession code 1FJG). b) All atoms RMSD deviations with respect to the initial X-ray (black) and NMR (grey) experimental structures along the simulation. The two terminal base-pairs at each end of the RNA fragment and the flipped out A1492 and A1493 residues were not included in the RMSD calculations.

Interestingly, both simulations predict a similar degree of conformational restriction in the oligosaccharide upon binding to its target RNA fragment. Figure 14 shows the experimental ensemble corresponding to neomycin B in the free state (obtained from the MD-tar simulations) in comparison with a theoretical ensemble corresponding to the antibiotic in complex with RNA (obtained from the MD simulations that started from both the X-ray and NMR coordinates). Distribution of ϕ(solid) and ψ(dotted) angles in both states are shown for the three glycosidic linkages (from top to bottom, Glc/Strp, Rib/Strp and Ido/Strp). These distributions were employed to evaluate the contribution ($-T\Delta S$) that rigification of every glycosidic linkage has to the global ΔG at 300 K. The $-T\Delta S$ values obtained are shown in Table 2. According to these data, a significant lost of conformational freedom upon binding is predicted mainly for the Rib/Strp and Glc/Strp linkages with $-T\Delta S$ values of around 1 kcal mol^{-1} per linkage at 300 K. A slightly lower contribution (0.5–0.8 kcal mol^{-1}) is predicted for the Ido/Strp bond. In fact both X-ray and NMR data indicate that this sugar fragment retains a significant internal mobility in the RNA bound state. Taking in account the three linkages the entropic cost associated to the ligand conformational freezing is in the 2.4–3.0 kcal mol^{-1} range. Obviously, this value constitute a lower limit as only a few degrees of freedom (ϕ/ψ angles) has been taken in account. Thus, conformational restriction of the hydroxymethyl groups upon binding probably makes also a significant contribution to the global ΔG. From the experimental distribution corresponding to the ribose hydroxymethyl in the free state (obtained from the MD-tar data) and those derived from the MD simulations of the complex an additional $-T\Delta S$ contribution of 0.7–1.0 kcal mol^{-1} at 300 K was estimated. Interestingly, according to both the X-ray and NMR structures of the complex, the OH6 of both Glc and Ido moieties are also involved in RNA recognition. Assuming a similar contribution to that estimated for the Rib hydroxymethyl group the total contribution that neomycin rigidification has to $\Delta G_{binding}$ is probably larger than 4–5 kcal mol^{-1}.

Conclusion

Herein, we demonstrate unambiguously that in solution the conformational behavior of the branched oligosaccharide antibiotic neomycin B is characterized by a remarkable flexibility with different conformations, even non-*exo*-anomeric ones, in fast exchange. This unusual behavior is related to the existence of branching. Here, polar contacts between non-vicinal sugar units leads to an enhanced flexibility of the Ribose glycosidic torsion

Our results suggest that freezing of the aminoglycoside upon binding to its target RNA makes a very significant contribution to the global ΔG of the process. This result opens the door to the design of neomycin conformationally constrained analogues able to bind RNA with a lower entropic penalty.

Experimental Section

Atomic charges for neomycin B were derived from HF/6-31G(d) ESP calculations using the Gaussian-94[20] program. This program was also used for the B3LYP/6-31G(d,p) optimizations. All MD simulations were carried out using the sander module within the AMBER 5.0 package[12] and the Cornell et al. force field.[19] Parameters for the acetalic functions were taken from GLYCAM.[21] Minimized neomycin B geometries were employed as starting structures for the simulations corresponding to the free state. The starting structures for the sugar/RNA complex were built from those reported for the paromomycin/A-site complex derived by both X-ray (pdb accession code 1FJG) and NMR methods (pdb accession code 1PBR). Solvated unconstrained simulations corresponding to both free and bound state and MD-tar simulations including only *J* information were carried out employing the following protocol. First, the free or complexed oligosaccharide was immersed in a bath of 2000–3200 TIP3P water molecules[17]

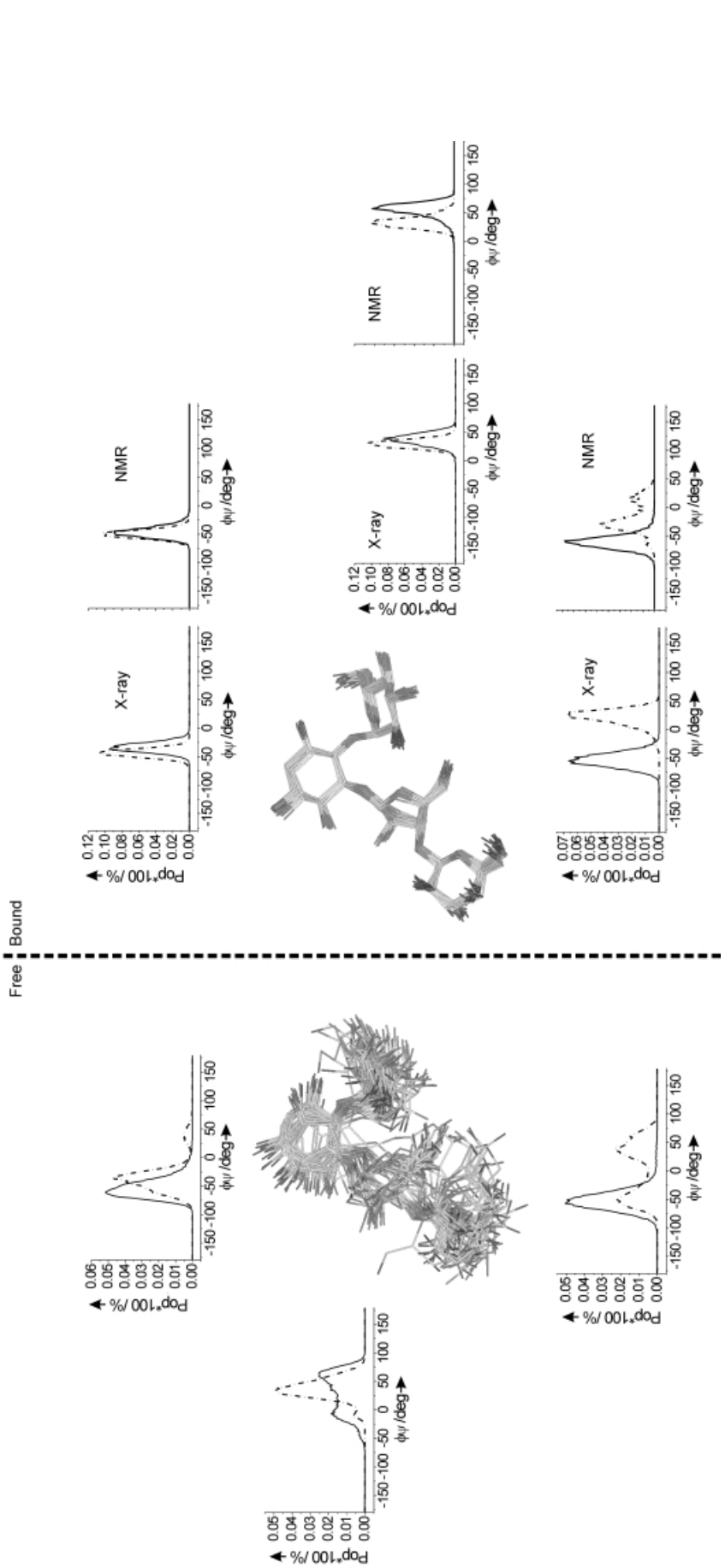

Figure 14. Experimental ensemble corresponding to neomycin B in the free state (obtained from the MD-tar simulations) in comparison with a theoretical ensemble corresponding to the antibiotic in complex with RNA obtained from the MD simulations (starting from both X-ray and NMR coordinates). Distribution of ϕ (——) and ψ (••••) rotamers in both states are shown for the three glycosidic linkages (from top to bottom, Glc/Strp, Rib/Strp and Ido/Strp). According to this data, rigidification of the sugar moiety upon binding should make a significant contribution to the entropic barrier of the recognition process.

0947-6539/02/0822-5238 $ 20.00+.50/0 *Chem. Eur. J.* **2002**, *8*, No. 22

Table 2. Entropy penalties associated to the freezing of the glycosidic (ϕ) and aglyconic (ψ) torsion angles of Neomycin-B upon binding to the decoding region aminoacyl-tRNA site (A site), for each glycosidic linkage.[a]

Linkage		S_{free}	S_{bound} (X-ray)	ΔS	$-T\Delta S$ [kcal mol^{-1}] (torsion)	$-T\Delta S$ [kcal mol^{-1}] (linkage)	S_{bound} (NMR)	ΔS	$-T\Delta S$ [kcal mol^{-1}] (torsion)	$-T\Delta S$ [kcal mol^{-1}] (linkage)
Glc/Strp	ϕ	6.92	5.62	−1.30	0.39	1.04	5.83	−1.09	0.33	0.95
	ψ	7.56	5.39	−2.17	0.65		5.49	−2.07	0.62	
Rib/Strp	ϕ	8.25	6.06	−2.19	0.66	1.18	6.30	−1.95	0.59	0.93
	ψ	7.16	5.44	−1.72	0.52		6.02	−1.14	0.34	
Ido/Rib	ϕ	7.09	6.39	−0.70	0.21	0.82	6.32	−0.77	0.23	0.51
	ψ	8.59	6.55	−2.04	0.61		7.66	−0.93	0.28	
total ϕ,ψ						3.04				2.39

[a] Conformational entropies for the free state were derived from the MD-tar distributions. Conformational entropies for the bound state were obtained from unrestrained MD simulations of the sugar/RNA complex employing both the X-ray (left) or the NMR (right) structures as starting coordinates. Total ΔS is probably higher due to the additional freezing of the hydroxymethyl groups.

(for the free and bound state, respectively) and neutralized with Na^+ (for the complexed state) or Cl^- (for the free state) ions using standard parameters for the Cornell et al. force field.[19] These ions were placed in the most favorable locations by using Coulombic potential terms with the LEAP module.[22] All simulations were performed using periodic boundary conditions and the particle-mesh Ewald approach[16] to introduce long-range electrostatic effects. The SHAKE algorithm[23] for hydrogen atoms, which allows the use of 2 fs time step, was employed. Finally, a 9 Å cutoff was applied to Lennard-Jones interactions.

Equilibration of the system was carried out as follows in all cases; as a first step, a short minimization with positional restraints on solute atoms was run to remove any potentially bad contact. The force constant for the positional constraints was 500 kcal mol^{-1} Å. We ran then a 12.5 ps molecular dynamics calculation at 300 K maintaining positional restraints on the sugar or sugar/RNA complex in order to equilibrate the water box and ions. For these two steps, a 9 Å cut-off was used for the treatment of the electrostatic interactions. As a next step, the system was equilibrated using the mesh Ewald method, as water properties are slightly different with this treatment i.e., density, average water–water energy and water diffusion values are slightly lower. With this purpose, a short MD simulation (12.5 ps) was run at 300 K, also using the Ewald approach for long-range electrostatic effects. Then, the system was subjected to several minimization cycles (each using 1000 steepest descent iterations) gradually reducing positional restraints on the sugar or sugar/RNA complex from 500 kcal mol^{-1} Å to 0. Finally, unrestrained MD trajectories at constant pressure (1 atm) and temperature (300 K) were collected and analyzed using the Carnal program.[24] Simulation lengths were 10 and 5 ns for unconstrained free and bound simulations, respectively and 1 ns for MD-tar simulations including only *J* infomation.

In addition, "in vacuo" 80 ns MD-tar simulations were performed including 14 NOEs and 5 *J* values corresponding to the ribose ring for the protonated state (pH 4.7) and 13 NOEs and five *J* for the neutral state (pH 9.7). For the protonated state different trajectories were collected both without charges and with charges ($\varepsilon = 4r$ and $\varepsilon = 80$). NOE-derived distances were included as time-averaged distance constraints and scalar coupling constants as time averaged *J* coupling restraints. A $\langle r^{-6}\rangle^{-1/6}$ average was used for the distances and a linear average was used for the coupling constants. The *J* values are related to the torsion τ by the well known Karplus relationship:[25]

$$J = A\cos^2(\tau) + B\cos(\tau) + C$$

The *A*, *B* and *C* values were chosen to fit the extended Karplus–Altona relationship for every particular torsion. At the end of the simulations the averaged *J* values were calculated using both the regular Karplus and the complete Altona equations and compared with the experimental ones.

Trial simulations were run using different simulation lengths (between 1 and 80 ns) and different force constants for the distances (between 10 and 30 kcal mol^{-1} Å^2) and *J* coupling constants (between 0.1 and 0.3 kcal mol^{-1} Hz^2) constraints. Different values for the exponential decay constant (between 100 ps and 8 ns) were also tested. These preliminary runs showed that for this flexible molecule, the use of exponential decay constants shorter than 1 ns produced unstable trajectories and led in some cases to severe distortions of the sugar rings. In contrast, good results were obtained when using exponential decay constant values of 5 ns or larger. It has been estimated that simulation lengths of ca. one order of magnitude larger than the exponential decay constant should be used to generate reliable estimates of average properties.[26] Thus, the final trajectories were run using an exponential decay constant of 8 ns and a simulation length of 80 ns.

It is also known that when using large force constants for the *J* coupling constraints, the molecule can get trapped in high energy, physically improbable, incorrect minima.[27] In order to solve this *false* minima problem, low values (between 0.1 and 0.3 kcal mol^{-1} Hz^2) were used for the *J* coupling restraints force constants.

Two final 80 ns MD-tar simulations (starting from different low energy conformations) were run. Population distributions obtained starting from different initial geometries were almost identical indicating that the simulation length is adequate for a proper convergence of the conformational parameters. Average distance and *J* values obtained in this way were found to correctly reproduce the experimental ones.

Entropy penalties associated to the freezing of the glycosidic (ϕ) and aglyconic (ψ) torsion angles of neomycin B upon binding to the decoding region aminoacyl-tRNA site (A-site) were calculated for each glycosidic linkage. Thus, conformational entropies for the free state were derived from the MD-tar distributions employing the expression $\Delta S = -R\Sigma P \ln P$. In a similar way, conformational entropies for the bound state were obtained from unrestrained MD simulations of the sugar/RNA complex employing both the X-ray (left) or the NMR (right) structures as starting coordinates.

NMR experiments: The NMR experiments were recorded on a Varian Unity 500. Selective 1D NOE experiments employed the 1D-DPFGSE NOE pulse sequence. NOEs intensities were normalized with respect to the diagonal peak at 0 mixing time. Selective T1 measurements were performed on the anomeric and several other protons to get the above mentioned value. Experimental NOEs were fitted to a double exponential function, $f(t) = p0(1 - e^{p2t})(1 - e^{p1t})$ with p0,p1 and p2 being adjustable parameters.[28] The initial slope was determined from the first derivative at time $t = 0$, $f'(0) = p0p1$. From the initial slopes interproton distances *r* were obtained by employing the isolated spin pair approximation.

Acknowledgement

Financial support from DGES (grants BQU2001-3693-C02-02 and BQU-2000-1501-C01) is acknowledged. We also thank the CAI of NMR of Universidad Complutense.

[1] *Glycosciences*: *Status and Perspectives* (Eds.: H. J. Gabius, S. Gabius), Chapman & Hall, London, **1997**.

[2] M. L. Philips, E. Nudelman, F. C. A. Gaeta, M. Perez, K. Singhal, S. Hakomori, J. C. Paulson, *Science* **1990**, *250*, 1130–1132.

[3] a) J. F. Espinosa, J. Cañada, J. L. Asensio, H. Dietrich, M. Martín-Lomas, R. R. Schmidt, J. Jiménez-Barbero, *Angew. Chem.* **1996**, *108*, 323–326; *Angew. Chem. Int. Ed. Engl.* **1996**, *35*, 303–306; b) J. F. Espinosa, E. Montero, A. Vian, J. Garcia, H. Dietrich, M. Martín-Lomas, R. R. Schmidt, A. Imberty, J. Cañada, J. Jiménez-Barbero, *J.*

  0947-6539/02/0822-5239 $ 20.00+.50/0

Am. Chem. Soc. **1998**, *120*, 10862 – 10871; c) M. J. Milton, D. R. Bundle, *J. Am. Chem. Soc.* **1998**, *120*, 10547 – 10548; d) A. Garcia, E. Montero, J. L. Muñoz, J. F. Espinosa, A. Vian, J. L. Asensio, F. J. Cañada, J. Jimenez-Barbero, *J. Am. Chem. Soc.* **2002**, *124*, 4804 – 4810.
[4] J. Dabrowski, T. Kozar, H. Grosskurth, N. E. Nifantév, *J. Am. Chem. Soc.* **1995**, *117*, 5534 – 5539.
[5] C. Landersjo, R. Stenutz, G. Widmalm, *J. Am. Chem. Soc.* **1997**, *119*, 8695 – 8698.
[6] F. Walter, Q. Vicens and E. Westhof, *Curr. Opin. Chem. Biol.* **1999**, *3*, 694 – 704.
[7] D. Fourmy, M. I. Recht, A. C. Blanchard, J. D. Puglisi, *Science* **1996**, *274*, 1367 – 1371.
[8] A. P. Carter, W. M. Clemons, D. E. Brodersen, R. J. Morgan-Warren, B. T. Wimberly, V. Ramakrishnan, *Nature* **2000**, *407*, 340 – 348.
[9] J. M. Ogle, D. E. Brodersen, W. M. Clemons, M. J. Tarry, A. P. Carter, V. Ramakrishnan, *Science* **2001**, *292*, 897 – 902.
[10] T. Hermann, E. Westhof, *J. Med. Chem.* **1999**, *42*, 1250 – 1261.
[11] D. A. Pearlman, *J. Biomol. NMR* **1994**, *4*, 1 – 16.
[12] D. A. Pearlman, D. A. Case, J. W. Caldwell, W. S. Ross, T. E. Cheatham, S. DeBolt, D. Ferguson, G. Siebal, P. Kollman, *Comp. Phys. Commun*. **1995**, *91*, 1 – 41.
[13] J. L. Asensio, A. García, M. T. Murillo, A. Fernández-Mayoralas, F. J. Cañada, C. R. Johnson, J. Jiménez-Barbero, *J. Am. Chem. Soc.* **1999**, *121*, 11318 – 11331.
[14] For detailed computational calculations on furanose moieties, see: a) M. T. Gordon, T. L. Lowary, C. M. Hadad, *J. Am. Chem. Soc.* **1999**, *121*, 9682 – 9692; b) T. J. Church, I. Carmichael, A. S. Serianni, *J. Am. Chem. Soc.* **1997**, *119*, 8645 – 8653; c) A. D. French, M. K. Dowd, P. J. Reilly, *J. Mol. Struct. (THEOCHEM)* **1997**, *271*, 395 – 396; d) S. Cros, A. Imberty, N. Bouchemal, C. Herve du Penhoat, S. Perez, *Biopolymers* **1994**, *34*, 1433 – 1441.
[15] a) Q. Xu, R. Gitti, C. A. Bush, *Glycobiology* **1996**, *6*, 281 – 288; b) K. E. Miller, C. Mukhopadhyay, P. Cagas, C. A. Bush, *Biochemistry* **1992**, *31*, 6703 – 6709.
[16] N. Navarre, N. Amiot, A. H. van Oijen, A. Imberty, A. Poveda, J. Jiménez-Barbero, M. A. Nutley, G. J. Boons, *Chem. Eur. J.* **1999**, *5*, 2281 – 2294.
[17] M. Chiansan, N. A. Baner, J. Simpson, J. A. McCammon, *J. Am. Chem. Soc.* **2002**, *124*, 1438 – 1442.
[18] C. S. A. T. Darden, *Annu. Rev. Biophys. Biomol. Struct.* **1999**, *28*, 155.
[19] W. D. Cornell, P. C. Cieplack, I. Bayly, I. R. Gould, K. Merz, D. M. Ferguson, D. C. Spellmeyer, T. Fox, J. W. Caldwell, P. A. Kollman, *J. Am. Chem. Soc.* **1995**, *117*, 5179 – 5197.
[20] *Gaussian 94*, Revision D.4, M. J. Frisch, G. W. Trucks, H. B. Schlegel, P. M. W. Gill, B. G. Johnson, M. A. Robb, J. R. Cheeseman, T. Keith, G. A. Petersson, J. A. Montgomery, K. Raghavachari, M. A. Al-Laham, V. G. Zakrzewski, J. V. Ortiz, J. B. Foresman, J. Cioslowski, B. B. Stefanov, A. Nanayakkara, M. Challacombe, C. Y. Peng, P. Y. Ayala, W. Chen, M. W. Wong, J. L. Andres, E. S. Replogle, R. Gomperts, R. L. Martin, D. J. Fox, J. S. Binkley, D. J. Defrees, J. Baker, J. P. Stewart, M. Head-Gordon, C. Gonzalez, J. A. Pople, *Gaussian Inc.*, Pittsburgh, PA, **1995**.
[21] R. J. Woods, R. A. Dwek, C. J. Edge, D. Fraser-Reid, *J. Phys. Chem.* **1995**, *99*, 3832 – 3839.
[22] C. E. A. F. Schafmeister, W. F. Ross, V. Romanovsky, University of California, San Francisco **1995**.
[23] J. P. Rykaert, G. Ciccote, J. C. Berendsen, *J. Comp. Phys.* **1977**, *23*, 327 – 334.
[24] W. S. Ross, *Carnal*: *Coordinate Analysis Program*, University of California, San Francisco, Department of Pharmaceutical Chemistry.
[25] For the relation between H/H couplings and conformation, see: a) M. Karplus, *J. Chem. Phys.* **1959**, *30*, 11 – 20; b) C. A. G. Haasnoot, F. A. A. M. de Leeuw, C. Altona, *Tetrahedron* **1980**, *36*, 2783 – 2794.
[26] A. E. Torda, R. M. Scheek, W. F. van Gunsteren, *Chem. Phys. Lett.* **1989**, *157*, 289 – 294.
[27] D. A. Pearlman, *J. Biomol. NMR* **1994**, *4*, 279 – 299.
[28] T. Haselhorst, T. Weimar, T. Peters, *J. Am. Chem. Soc.* **2001**, *123*, 10705 – 10714.

Received: June 19, 2002 [F4192]

  0947-6539/02/0822-5240 $ 20.00+.50/0